



Contents lists available at ScienceDirect

Journal of Quantitative Spectroscopy and Radiative Transfer

journal homepage: www.elsevier.com/locate/jqsrt

Line shape parameters of self-broadened CO transitions in the (3-0) overtone band

Q. Huang^a, J. Wang^c, J.-K. Li^a, Z.-L. Nie^a, A.-W. Liu^{b,c}, Y. Tan^{a,c}^{*}, S.-M. Hu^{a,c}^a Hefei National Research Center of Physical Sciences at the Microscale, University of Science and Technology of China, Hefei, 230026, Anhui, China^b State Key Laboratory of Molecular Reaction Dynamics, Department of Chemical Physics, University of Science and Technology of China, Hefei, 230026, Anhui, China^c Hefei National Laboratory, University of Science and Technology of China, Hefei, 230088, Anhui, China

ARTICLE INFO

Keywords:

Carbon monoxide

Cavity ring-down spectroscopy

Line broadening parameters

ABSTRACT

This study employs laser-locked cavity ring-down spectroscopy to investigate 15 weak $^{12}\text{C}^{16}\text{O}$ transitions in the near-infrared, corresponding to the P and R branches of the (3-0) band with rotational quantum numbers J ranging from 25 to 35. Most spectra were recorded at low pressures (below 1333 Pa), where Doppler broadening dominates, and collision broadening is mainly driven by speed-dependent interactions. This environment enables precise determination of collisional line shape parameters. The Padé approximation and polynomial fit were used to estimate speed-dependent Voigt (SDV) broadening parameters, extending the data to higher rotational quantum numbers. Accurate self-broadening parameters for CO were obtained, which are essential for studying pressure broadening by other atmospheric gases. These results will support high-precision radiative transfer models for Earth's atmosphere in this spectral region.

1. Introduction

Carbon monoxide plays a significant role as a greenhouse gas. It contributes to the trapping of infrared radiation, which raises Earth's surface temperature and also engages in atmospheric chemical reactions, such as diminishing OH radical levels. This prolongs the existence of other greenhouse gases like CO_2 and CH_4 , intensifying global warming [1]. Moreover, carbon monoxide is a crucial pollutant in the atmosphere, influencing regional air quality and public health, while also serving as an indicator for the long-range transport of human-made pollutants [2]. In addition, carbon monoxide is one of the key molecules in interstellar research, second only to hydrogen in abundance [3]. Within our solar system, it is a vital component of planetary atmospheres, like those of Venus [4,5] and Mars [6,7]. The investigation of carbon monoxide typically targeted the fundamental (1-0) band near 4.7 μm . In contrast, the second overtone (3-0) in the near-infrared was less investigated due to its substantially diminished line strength, being four orders of magnitude weaker than the (1-0) band. The (3-0) band, located around 1.6 μm , plays a crucial role in atmospheric detection and remote sensing applications. Analyzing the line shape parameters of the (3-0) band enhances the precision of modeling Earth's atmospheric radiation transfer. Wójtewicz et al. [8] utilized frequency-stabilized CRDS spectroscopy to precisely gauge the spectral line profile parameters of self-broadened carbon monoxide

(3-0) and (4-1) band transitions, achieving high sensitivity and high spectral resolution at low pressures. Borkov et al. [9] employed Fourier transform spectroscopy to measure the CO absorption spectrum across the wavenumber range 6000–6450 cm^{-1} , focusing on the line strengths and self-broadening coefficients of six isotopologues' (3-0) bands and the hot (4-1) band of $^{12}\text{C}^{16}\text{O}$. Hashemi et al. [10] have updated and expanded the spectral line shape parameters for the CO molecule in the HITRAN2020 database [11]. They compared and analyzed the existing experimental data using the Voigt and speed-dependent Voigt (SDV) line shape functions. Furthermore, they employed the Padé approximation model to analyze the data, thereby determining the self-broadening parameters of carbon monoxide. Bielska et al. [12] conducted an analysis of the line strength of the second overtone band (3-0) of CO in the near-infrared, obtaining results with exceptional precision and accuracy. Their findings demonstrated consistency between measured data and theoretical predictions, with discrepancies under 1%, confirming the validity of both experimental and theoretical models for line strength predictions. Our group's previous work also achieved certain research findings in the high-precision measurement of carbon monoxide spectral line parameters around 1.56 μm , mainly focusing on the line frequency [13–15]. And in the latest study, our team has also reported simultaneous measurements of cavity-enhanced absorption and dispersion spectroscopy on the prototype molecule $^{12}\text{C}^{16}\text{O}$,

* Corresponding author.

E-mail address: tanyan@ustc.edu.cn (Y. Tan).<https://doi.org/10.1016/j.jqsrt.2025.109483>

Received 17 December 2024; Received in revised form 16 April 2025; Accepted 18 April 2025

Available online 6 May 2025

0022-4073/© 2025 Published by Elsevier Ltd.

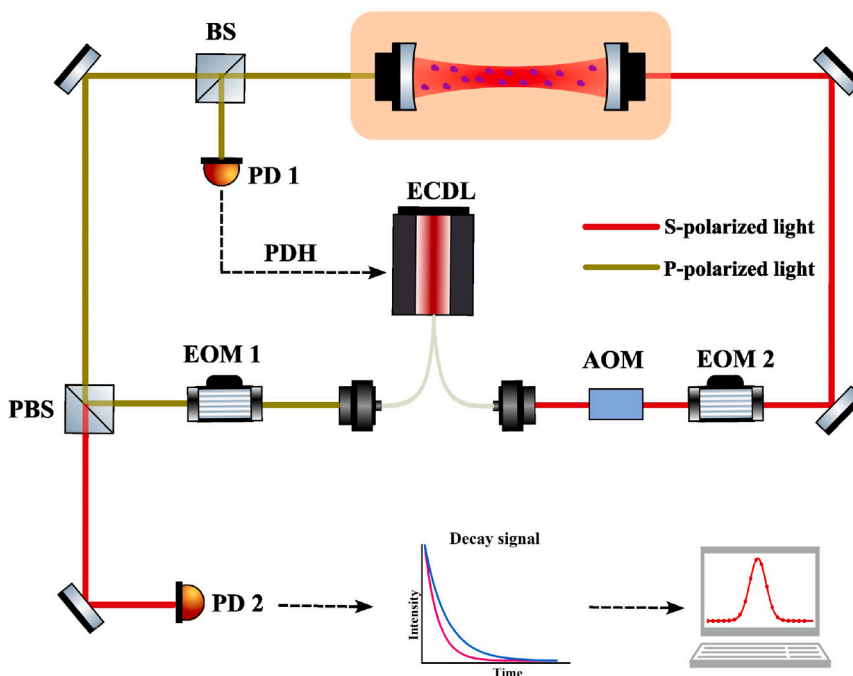


Fig. 1. Configuration of the experimental setup for cavity ring-down spectroscopy (CRDS). Abbreviations: AOM, acousto-optic modulator; BS, beam splitter; ECDL, external-cavity diode laser; EOM, electro-optic modulator; PBS, polarizing beam splitter; PD, photodiodes.

utilizing the same optical resonant cavity. Measurements were taken on nine lines within the R branch of the (3-0) band, and concentrated on the line intensities with an experimental uncertainty of approximately 1‰ [16]. Building upon prior research, this investigation employs laser-locked cavity ring-down spectroscopy (LL-CRDS) to examine 15 weak transitions of CO in the near-infrared. These correspond to the P and R branches of the (3-0) band with rotational quantum numbers $J \geq 25$. The experiments were performed at low pressures, all under 1333 Pa, where Doppler broadening is dominant and collision broadening arises primarily from speed-dependent interactions. This allows for the determination of more precise collisional line shape parameters through spectral line shape fitting. Moreover, we applied Padé approximation to estimate the SDV profile broadening parameters for CO molecular absorption spectra, together with previously reported values in the literature. This enabled us to extend the experimental results to higher rotational quantum numbers. The primary aim of this research is to acquire highly precise self-broadening line shape parameters for CO, which are vital for subsequent investigations of CO pressure broadening by other atmospheric gases, as self-broadening must also be considered. This study will contribute to future high-precision radiative transfer simulations in this spectral region of Earth's atmosphere.

2. Experimental details

In this study, we employed a Laser-locked cavity ring-down spectroscopy technique [17] to record the spectra of the CO (3-0) vibrational band near 1560 nm. Fig. 1 provides a schematic depiction of the experimental setup. The optical cavity was composed of two mirrors with a reflectivity of 99.997%, functioning in the 1.5–1.7 micrometer wavelength range. The cavity was around 118 cm long, resulting in a free spectral range (FSR) of about 126.9 MHz. The width of the cavity mode was approximately 0.6 kHz. The employed light source was an External Cavity Diode Laser (ECDL, Toptica). The laser light emitted was split into two orthogonally polarized beams before they were coupled into the optical cavity. These beams entered the cavity from different sides. One of these beams, known as the “locking beam”, was employed to synchronize the laser frequency with the cavity mode

and was stabilized using the Pound–Drever–Hall (PDH) technique. This method enhanced the stability of the laser frequency and narrowed the laser line-width, thereby facilitating better coupling of light into the cavity. The second beam, referred to as the “probing beam”, underwent frequency modulation employing an acousto-optic modulator (AOM) along with an electro-optic modulator (EOM). Frequency adjustment was accomplished by modifying the radio frequency applied to the EOM. When the frequency of the probe beam, modulated by both the AOM and EOM, coincided with a longitudinal mode of the optical cavity, the photodiode was able to detect the transmitted light within the cavity. All radio frequencies were synchronized using a GPS-synchronized rubidium clock (SRS FS725).

3. Retrieval of the spectral line parameters

The rovibrational lines from the P and R branches of the (3-0) band for CO were measured using a carbon monoxide sample that had a purity level of 99.99%. And we used a carbon monoxide sample with a known isotopic abundance, in which the abundance of the main isotope $^{12}\text{C}^{16}\text{O}$ is 0.98699 [16]. Each line was measured at numerous pressures between 0 and 1333 Pa. The rotational quantum numbers J of these spectral lines lie within the range of 25 to 35. The obtained spectra were analyzed using the Hartmann-Tran profile (HTP) [18,19], which incorporates seven parameters: the Doppler half-width Γ_D , the pressure-induced half-width Γ_0 , the speed-dependent relaxation rate Γ_2 , the pressure-induced line shift Δ_0 , the speed-dependent line shift Δ_2 , the velocity-changing collisions ν_{vc} , and the correlation parameter η . During the fitting of each spectrum captured through CRDS, the Doppler half-width was fixed to the calculated value of the corresponding experimental temperature.

The HTP simplifies to a Voigt profile when the parameters Γ_2 , Δ_0 , Δ_2 , ν_{vc} , and η are all set to zero. Similarly, it reduces to an SDV profile under the condition that Δ_0 , Δ_2 , ν_{vc} , and η are zero. As illustrated in Fig. 2, we analyzed the experimentally obtained absorption spectra using three distinct profiles: the Voigt profile (VP), the speed-dependent Voigt profile, and the Hartmann-Tran profile (HTP). These were applied to the R(26) line at 365 Pa and P(35) line at 1216 Pa and 9111 Pa of $^{12}\text{C}^{16}\text{O}$. To assess the fit quality for the R(26) line and P(35) line, the

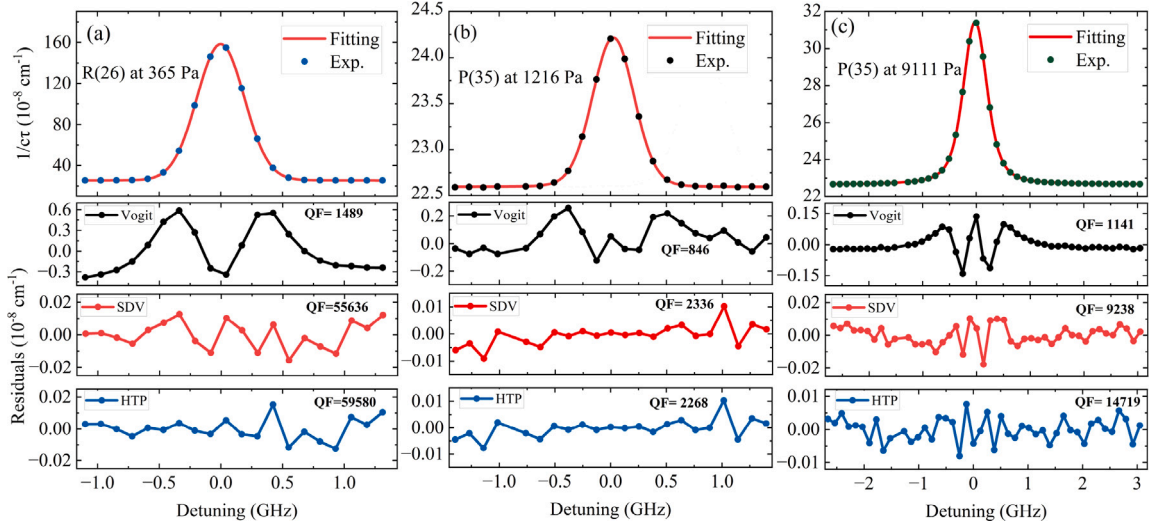


Fig. 2. The R(26) line at 365 Pa and P(35) line at 1216 Pa and 9111 Pa of $^{12}\text{C}^{16}\text{O}$ were evaluated through a single scan at 299 K. The top panel displays the absorption spectrum with measured data (symbols) overlaid by the fit (line). The bottom panels illustrate the fit residuals and QF values for the specified profiles.

quality of fit (QF) parameter was used, providing a means to evaluate how well the different line profiles matched the spectra. QF is defined as [20]:

$$\text{QF} = \alpha_c / \sigma \quad (1)$$

where α_c is the absorption coefficient at the center of the absorption peak, and σ is the standard deviation of the fitting residuals, calculated as:

$$\sigma = \sqrt{\frac{\sum_{i=1}^M (\alpha^{\text{exp}}(v_i) - \alpha^{\text{simu}}(v_i))^2}{M - k}} \quad (2)$$

where $\alpha^{\text{exp}}(v_i)$ and $\alpha^{\text{simu}}(v_i)$ are the experimental and simulated absorption coefficients at frequency v_i , respectively, v_i is the frequency of the i th cavity mode, M is the total number of spectral points, and k is the number of adjustable line shape parameters. QF assesses the quality of the spectral fit. It considers not only the random noise in the experimental spectrum but also the systematic distortion of the line shape. A larger QF value indicates smaller fitting residuals and thus better fit quality. The QF parameter can be used to compare the fitting effects of different line shape models and select the best line shape model. From the results shown in Fig. 2, it can be observed that the QF of the Voigt profile is significantly lower than those of the other two profiles, and the residuals at the peak center exhibit a ‘W’ shape. This effect is often attributed to line narrowing. The QFs of the SDV and HTP profiles are improved by 10 times or more compared to the Voigt profile, with only minimal differences between the SDV and HTP profiles. This is because the experimental pressures are relatively low, within 1333 Pa, where the influence of velocity-changing collisions and their correlation is minor. When the experimental pressure increases to approximately 10 kPa, the fitting residual of the SDV line shape becomes significantly worse compared to the HTP linear model. This is also evident from the QF values, where the QF of the HTP line shape increases by about 60% compared to that of the SDV line shape. This indicates that at higher pressures, the SDV line shape also exhibits its limitations, primarily due to the speed-dependent line shift and velocity-changing collisions under higher pressure. The HTP model appears to be a more suitable line shape choice under higher pressure conditions compared to the SDV model.

Fig. 3 illustrates the absorption spectra of R(26) and P(35) at 299 K, with the results fitted using the SDV line shape. The spectrum of R(26) was measured at pressures ranging from 123 Pa to 365 Pa. The spectrum of P(35) was recorded in two pressure ranges: one from 899 Pa to 1026 Pa and the other one from 9111 Pa to 11213 Pa.

This division was necessary because the P(35) line has the weakest absorption among the lines measured in this study, with a line strength of more than two orders of magnitude weaker than the R(26) line. The signal-to-noise ratio of the P(35) line at pressures of around 1 kPa was limited, leading to relatively large uncertainties in the values γ_0 and γ_2 , reaching approximately 3% and 8%, respectively. Consequently, in subsequent experiments, the measurement pressure was increased to 10 kPa to improve the accuracy of γ_0 and γ_2 . As shown in the bottom panel of Fig. 3, which presents the residuals of the fits, the residuals at different pressures are consistent. Although the SDV line shape fitting results for P(35) at high pressures are less accurate, this work focuses on the line parameters of the SDV profile. Therefore, the high-pressure data, which serves as a supplement, was also fitted with the SDV profile.

Fig. 4 illustrates the line broadening parameters Γ_0 and Γ_2 , which were derived from fitting CRDS spectra of the R(26) and P(35) lines observed at various pressures. Moreover, both Γ_0 and Γ_2 exhibit a strong linear relationship with pressure, and the broadening coefficients γ_0 and γ_2 were obtained through a linear fit of this data. For the R(26) line, the relative uncertainties in γ_0 and γ_2 are 2‰ and 12‰, respectively. For the P(35) line, after including the results from higher pressures, the relative uncertainties of γ_0 and γ_2 are reduced to 0.6‰ and 5‰ respectively. Despite the weaker absorption of P(35) compared to R(26), its broadening coefficients exhibit lower relative uncertainties. This improvement is attributed to the increased line broadening at higher pressures, which leads to smaller relative uncertainties. This research, conducted by measuring and fitting spectral data under various pressures, contributes significantly to a better understanding of the applicability and limitations of the SDV line shape under different conditions. By increasing the measurement pressure, more reliable line parameters can be obtained, which is crucial for accurate analysis. Additionally, this work provides important reference data for the application of the SDV line shape over a wider range of pressures.

Table 1 lists the parameters for a total of 15 lines in $^{12}\text{C}^{16}\text{O}$, including P(25) - P(35) and R(25) - R(32). The parameters include line positions (taken from our previous work [15]), self-broadening coefficients, and speed-dependent parameters along with their uncertainties. All measurements had been done at a temperature of 299 K. The collisional broadening coefficients were corrected to the reference HITRAN temperature of 296 K based on the power-law equation and the n_ν values provided by the HITRAN database [10]. From the table, it can be seen that the self-broadening parameter γ_0 from our experimental results is consistent with the HITRAN database [10], whereas γ_2 is

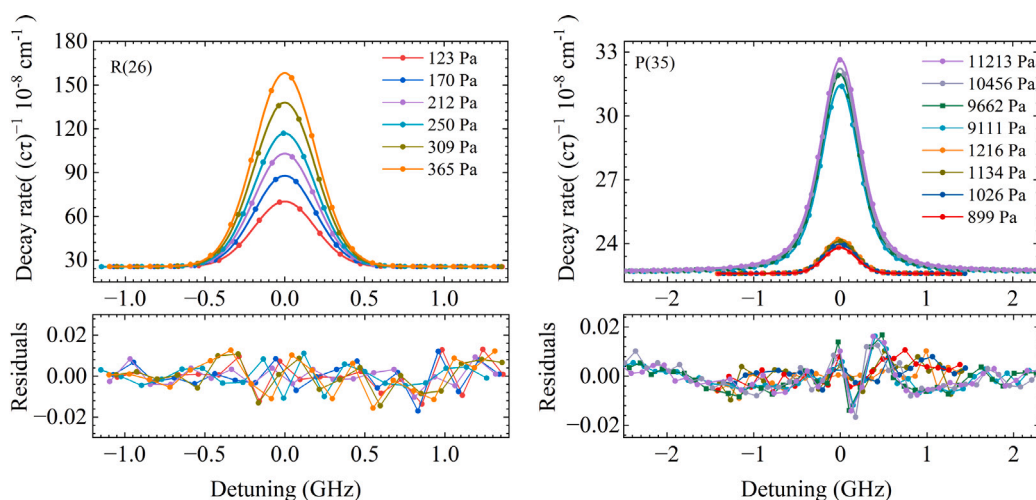


Fig. 3. Upper left panel: CRDS spectra for the R(26) line of $^{12}\text{C}^{16}\text{O}$ are shown, recorded at 299 K with a pure CO sample gas pressure ranging from 123 to 365 Pa. Upper right panel: The absorption spectrum of the P(35) line of CO at 299 K, with a pure CO sample gas pressure between 899 and 11213 Pa, is depicted. Dots represent the experimental data, while the solid lines correspond to the simulated spectra. Bottom panel: Displays the fitting residuals, using speed-dependent Voigt (SDV) profiles for the fit.

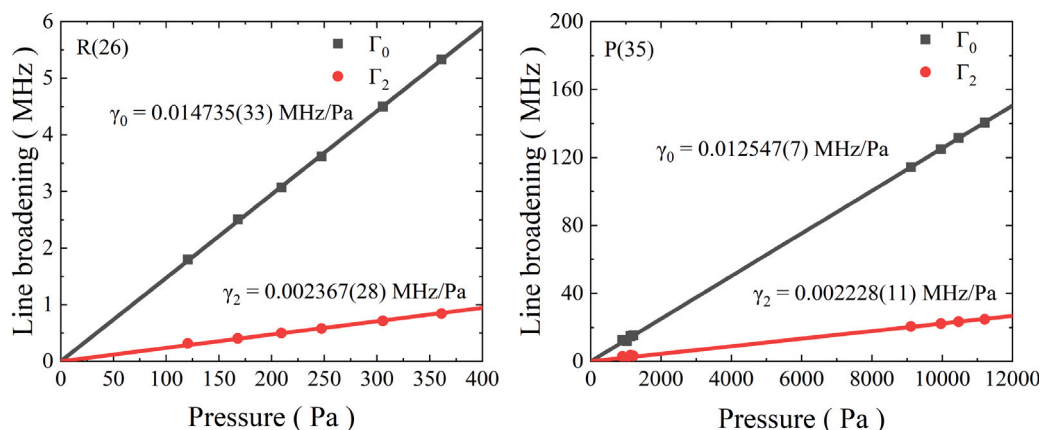


Fig. 4. Line broadening parameters Γ_0 and Γ_2 obtained from fitting CRDS spectra of the R(27) line (left panel) and P(35) line (right panel) recorded under different pressures. Speed-dependent Voigt (SDV) profiles were used in the fit. Coefficients γ_0 and γ_2 were determined by a linear fit of the data.

generally 2-3 times larger than the values taken from HITRAN2020. For these 15 carbon monoxide lines, the relative uncertainties of γ_0 and γ_2 were determined with uncertainties within 5‰ and 5%, respectively. In contrast, the relative uncertainties of γ_0 and γ_2 provided in the HITRAN 2020 database range between 5% and 10%. In the region of high J values, precise measurement of line parameters becomes particularly challenging. Our experimental results offer higher precision data in this area, which can serve as a significant supplement to the HITRAN2020 database [11], thereby enhancing the overall quality of the database. In this work, we did not use a frequency comb to calibrate the absolute frequency of the probing laser, so the horizontal axis of the spectrum we detected corresponds to relative frequency which including the center position of the spectral line and pressure shift. Since the δ_0 and δ_2 are coupled together, it is difficult to obtain the value of δ_2 in this work. Furthermore, in this work, the experimental pressure is very low, making the value of δ_2 very small and almost negligible. Therefore, we did not discuss the δ_0 and δ_2 parameters.

In this section, we examine the uncertainties associated with γ_0 and γ_2 derived from CRDS spectroscopy. The uncertainty analysis for the R(26) line serves as an illustrative example. The errors are classified into Type A and Type B. Table 2 provides a comprehensive error budget for the collisional broadening parameters of R(26). The overall uncertainty is calculated as $u_{tot} = (\sum u_i^2)^{1/2}$.

In this experiment, we utilized ultra-pure CO gas (from AirLiquid, with a reported purity exceeding 99.99%) as our sample gas. A cold

Table 1

The collisional broadening parameters from the SDV line shape fit ($\text{cm}^{-1}/\text{atm}$).

line	Position cm^{-1}	This work		HITRAN2020 [11]	
		$\gamma_0, \text{cm}^{-1}/\text{atm}$	$\gamma_2, \text{cm}^{-1}/\text{atm}$	$\gamma_0, \text{cm}^{-1}/\text{atm}$	$\gamma_2, \text{cm}^{-1}/\text{atm}$
P(35)	6139.473852	0.04270(2)	0.007581(40)	0.043	0.00264
P(33)	6168.986057	0.04331(14)	0.007617(311)	0.045	0.00285
P(32)	6176.114000	0.04495(16)	0.007580(317)	0.045	0.00291
P(31)	6183.141570	0.04537(18)	0.006904(401)	0.046	0.00297
P(30)	6190.068725	0.04692(24)	0.008097(80)	0.047	0.00303
P(27)	6210.245763	0.05037(11)	0.008175(26)	0.049	0.00324
P(25)	6223.192140	0.05141(15)	0.007908(109)	0.050	0.00339
R(25)	6413.122496	0.04957(12)	0.007090(100)	0.049	0.00331
R(26)	6414.080821	0.05015(11)	0.008054(95)	0.049	0.00324
R(27)	6414.930187	0.04915(12)	0.007974(90)	0.048	0.00317
R(28)	6415.670442	0.04817(14)	0.008281(70)	0.047	0.00310
R(29)	6416.301445	0.04778(5)	0.008382(25)	0.047	0.00303
R(30)	6416.823044	0.04688(30)	0.008468(137)	0.046	0.00297
R(31)	6417.235084	0.04598(4)	0.008593(26)	0.045	0.00291
R(32)	6417.537471	0.04513(9)	0.008608(50)	0.045	0.00285

trap maintained at liquid nitrogen temperature was employed to eliminate potential impurities prior to usage. The impact of the gas purity on the relative systematic errors of γ_0 and γ_2 is quantified as 0.1‰. Using CRDS absorption spectra, we quantified the concentrations of the three principal isotopologues, following the primary isotopologue

$^{12}\text{C}^{16}\text{O}$, within our gas sample: namely $^{13}\text{C}^{16}\text{O}$, $^{12}\text{C}^{18}\text{O}$, and $^{12}\text{C}^{17}\text{O}$. The relative measurement uncertainty for the isotopic concentration of $^{12}\text{C}^{16}\text{O}$ stands at 0.2‰ [16], contributing equally (0.2‰) to the relative systematic errors in γ_0 and γ_2 .

The pressure measurements were performed using a capacitance manometer (Leybold CTR101N), which, according to the manufacturer, provides an accuracy of 1.2‰ relative to the current reading. This device underwent several calibrations against an optical manometer possessing an accuracy of 0.012‰ ($k = 1$) [21]. Post-calibration, the 1σ variation in the pressure readings equaled 0.5‰, and this value is applied as the measurement uncertainty in our analysis [16]. The impact of these pressure measurements on the relative systematic uncertainty of γ_0 and γ_2 amounts to 0.5‰.

The stainless steel was employed in the construction of the external compartment of the sample cavity to ensure a vacuum environment. An integrated heating pad was attached to this steel surface to facilitate the initial management of temperature conditions. Throughout the measurement process, temperature variations were assessed using two SPRTs (model 5686-B, Fluke), strategically placed at opposite ends of the ring-down cavity. These sensors, along with the readout device (model MKT50, Anton Parr), underwent calibration at the National Institute of Metrology, Beijing, with an uncertainty margin of less than 5 mK. Over a 12-hour period, the sensors recorded a temperature drift, revealing that fluctuations were confined to approximately 1 mK, with deviations between the sensors remaining below 3 mK [16]. This stability affirms the temperature uniformity within the cavity. The resulting contributions to γ_0 and γ_2 from temperature readings are quantified at 0.9‰ and 2.8‰, respectively.

To evaluate systematic uncertainties associated with line shape, we compared γ_0 and γ_2 derived from fits using the SDV and HTP line shapes, respectively, noting relative uncertainties of 0.2‰ and 1.2‰. We further studied baseline selection effects on collisional broadening parameters, finding that the spectral baseline exhibited an etaloning effect with a periodicity of approximately 30 GHz. Over the spectral acquisition interval, the baseline showed a quasi-linear trend. We compared two baseline correction techniques: one using a fit with periodic etaloning components excluded, and another relying on standard linear fitting. The analysis determined that the variation in calculated collisional broadening parameters using these methods was limited to 0.2‰.

Presently, the dominant uncertainty source in collisional broadening remains the Type A uncertainty arising from statistical limitations. However, Type B uncertainties, predominantly contributed by systematic deviations in line profile characterization and temperature measurement determination, constitute the principal error component. Based on comprehensive error propagation analysis, we determined the total uncertainties for the R(26) transition parameters γ_0 and γ_2 to be 2.5‰ and 12.2‰, respectively. Furthermore, by systematically accounting for correlated errors in γ_0 and γ_2 , the derived a_w parameter was assigned a consolidated uncertainty of 12.4‰. Subsequent refinement of uncertainty budgets for both P- and R-branch transitions incorporated Type B systematic deviations to ensure rigorous error characterization.

4. Empirical model based on Padé approximation

We constructed a model aimed at characterizing the variation in line width as influenced by rotational quantum numbers, resulting from the self-collision of carbon monoxide molecules across different vibrational energy levels. To achieve this, we utilized both experimental and previously documented data from the literature. Initially, we compiled the available experimental information, categorizing it according to vibrational energy levels and rotational quantum numbers. Then, we employed the Padé approximation function to fit this data, yielding an expression that describes the relationship between line width and

Table 2

Error budget ($k = 1$) of the collision broadening parameters of R(26) (unit: permille, ‰).

Source	$u_r(\gamma_0)$	$u_r(\gamma_2)$	$u_r(a_w)$
Type A			
Statistical	2.2	11.8	12
Type B			
Sample gas purity	0.1	0.1	/
Isotopic abundance of $^{12}\text{C}^{16}\text{O}$	0.2	0.2	/
Temperature measurement accuracy	0.9	2.8	2.9
Pressure measurement accuracy	0.5	0.5	/
Line shape	0.2	1.2	1.2
Baseline	0.2	0.2	0.3
Total	2.5	12.2	12.4

rotational quantum numbers. Using the obtained fitting coefficients, we calculated the line width parameters for all CO molecule spectral lines.

The Padé approximation is a technique from numerical analysis for estimating the representation of functions. It has been incorporated into the empirical model for line-broadening parameters within the HITRAN database by Tan et al. [22]. This method's strength lies in its ability to maintain a smooth, asymptotic-like form when extrapolating to high rotational quantum numbers that go beyond experimental measurements, thereby avoiding major nonphysical discrepancies. It simplifies intricate functional forms by expressing a function as a ratio of two polynomials. The expression is presented as follows [10]: [10]:

$$\gamma = \frac{(c_0 + c_1 \times |m| + c_2 \times |m|^2 + c_3 \times |m|^3)}{(1 + d_1 \times |m| + d_2 \times |m|^2 + d_3 \times |m|^3 + d_4 \times |m|^4)} \quad (3)$$

In the equation, γ denotes the parameter associated with collisional broadening, while m signifies the modification in rotational quantum number J , with $m = -J$ for the P-branch and $m = J + 1$ for the R-branch. The terms c_0, c_1, c_2, c_3 and d_1, d_2, d_3, d_4 are coefficients in the Padé approximation formula, which are identified through fitting. By adjusting the coefficients c_0, c_1, c_2, c_3 and d_1, d_2, d_3, d_4 against experimental data, one can compute the collisional broadening parameters for various J values. The Padé approximation formula facilitates the extrapolation of experimental findings to higher J values, which is essential for the development of a more extensive molecular spectral database.

We compared the self-broadening parameters, γ_0 (SDV profile), for 15 spectral lines of the P and R branches of CO with previously reported results, as shown in Fig. 5, which includes the CO (0-0) [23], (2-0) [24], (3-0) [9,25,26], (4-0) [27], and (7-0) [28] bands. Due to the weak absorption measured by Balashov et al. [28] in the CO (7-0) band, their results exhibited an overall upward drift compared to other experimental results, with significant errors. Consequently, we decided to exclude this dataset when selecting data for fitting. Balashov's data were omitted from the fit but retained in Fig. 5 for comparative purposes to illustrate experimental discrepancies. We then used Eq. (3) for fitting. Since the values of $c_0, c_1, c_2, c_3, d_1, d_2, d_3,$ and d_4 in Eq. (3) are highly coupled in fitting, we iteratively alternated and fixed the values of these parameters for fitting. After approximately 200,000 iterations, the fitting results converge. The final fitting result is shown by the red solid line in Fig. 5, and it is compared with the literature by Hashemi et al. [10] (HITRAN2020 [11]). The specific fitting coefficients are given in Table 3. From the bottom panel of Fig. 5, in the region of the low rotational numbers $|m|$ values, our fitting results align well with those from HITRAN 2020, with deviations within 2%. As the m value increases, the deviation becomes larger, reaching approximately 4% smaller than the HITRAN 2020 results when the rotational numbers $|m|$ equals 40. The results presented in Hashemi et al. [10] were fitted solely to the data from Devi et al. [24], lacking information in the high $|m|$ value interval. Our work, however, supplements this gap in the high m region, enhancing the reliability of the fitting results. Within the $|m|$ interval, the standard deviation of the

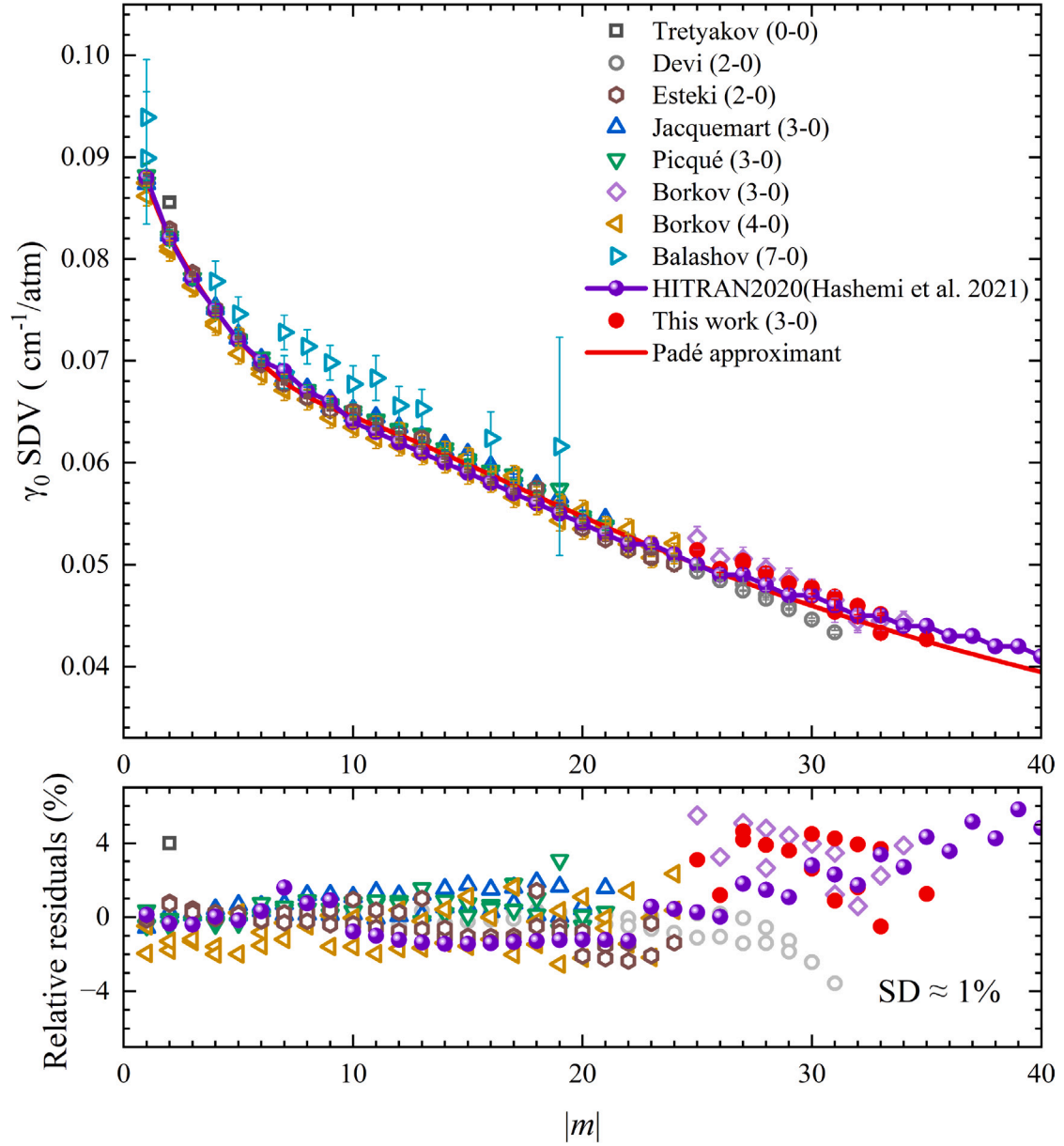


Fig. 5. Upper panel: A comparison of γ_0 (SDV) in units of $\text{cm}^{-1}/\text{atm}$ plotted against the rotational numbers $|m|$ is shown for several bands as reported by Tretyakov et al. [23], Devi et al. [24], Esteki et al. [29], Jacquemart et al. [25], Picqué et al. [26], Borkov et al. [9,27], Balashov et al. [28], and this study. The Padé fit excludes the Balashov et al. [28] CO (7-0) band data due to weak absorption-induced systematic drift. Bottom panel: The relative residuals from the Padé approximation are plotted.

Table 3

The coefficients obtained in fitting Eq. (3) and a third-order polynomial for calculating the self-broadening parameters, γ_0 (in $\text{cm}^{-1}/\text{atm}$), and the speed-dependent parameters, a_w , of CO at 296 K using the SDV profile.

The Padé approximation of γ_0			The third-order polynomial of a_w	
coef.	<i>This work</i>	Hashemi et al. [10]	coef.	<i>This work</i>
e_0	3.7835	-0.6002	A	0.15155
e_1	74.698	0.9753	B	-0.010438
e_2	-11.710	1.61	C	6.2762×10^{-4}
e_3	0.85843	1.25	D	-8.5854×10^{-6}
d_1	860.95	-1		
d_2	-97.475	19.99		
d_3	4.7237	16.42		
d_4	0.32083	0.3637		

relative residuals for γ_0 (SDV profile) from the Padé approximation is approximately 1%.

Fig. 6 shows the results of the speed-dependent parameters ($a_w = \gamma_2/\gamma_0$, SDV) for 15 spectral lines of the P and R branches of CO and previously reported results, including the CO pure rotational [30], (0-0) [23], (2-0) [24], (3-0) [8,9], (4-0) [27], and (7-0) [28] bands. The current values of the speed-dependent parameter (SDV profile) a_w for CO in Hashemi et al. [10] are based on the results of Devi et al. [24]. However, according to experimental findings from this work, the variation of a_w exhibits a certain deviation from the results in Hashemi et al. [10]. The larger the $|m|$ value, the larger the deviation from Hashemi et al. [10], with the maximum deviation exceeding three times the value. In the region of high $|m|$ values, our results show a good agreement and consistent trend with those of Borkov et al. [9]. In our work, we did indeed consider the uncertainties associated with the literature data when constructing the empirical models for the CO self-broadening parameters. We employed a weighted fitting approach, where each data point was assigned a weight based on the inverse of its squared uncertainty. This weighting scheme effectively reduced the influence of data points with larger uncertainties, ensuring that

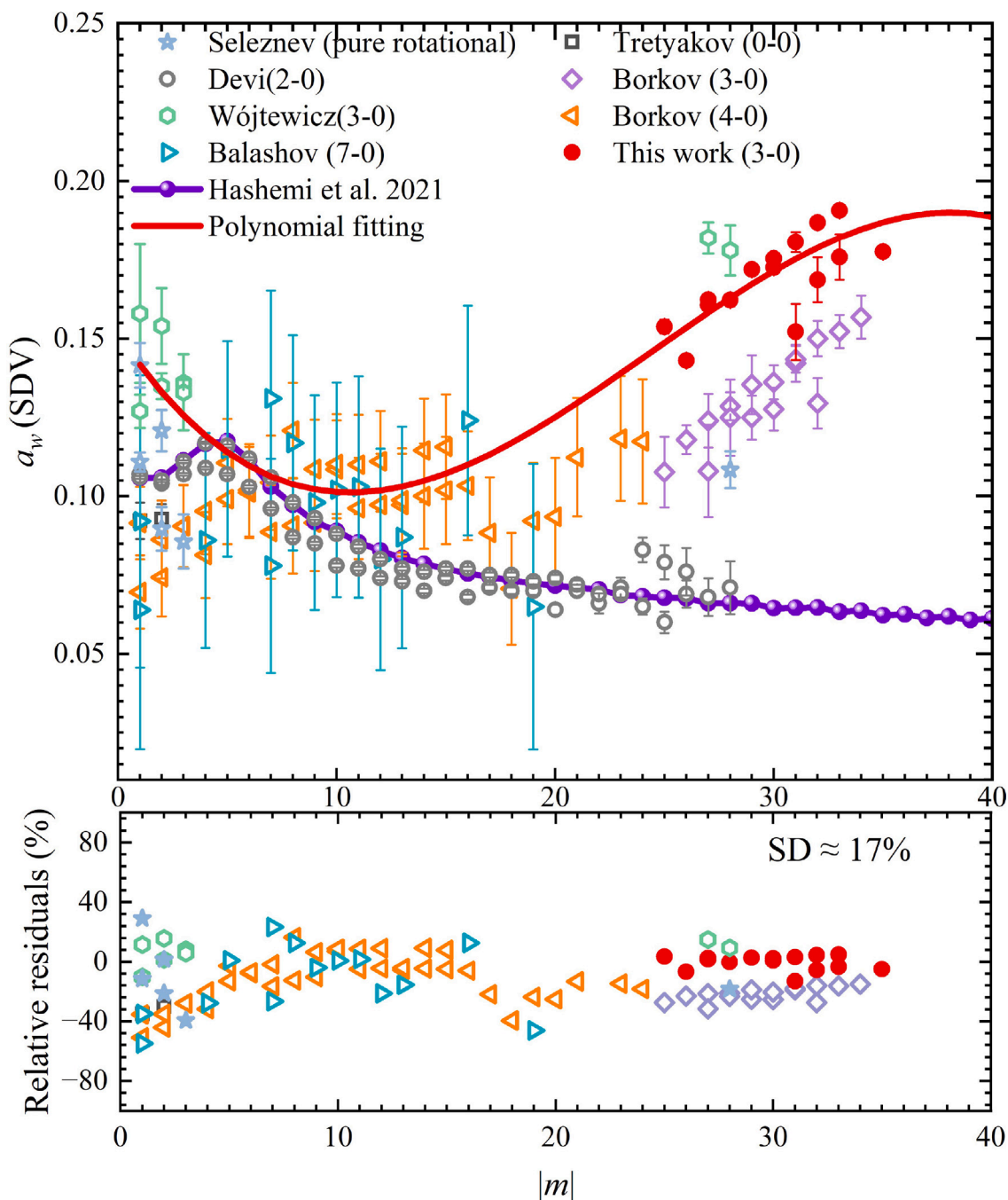


Fig. 6. Upper panel: The comparison of a_w (SDV profile, no unit) versus $|m|$ for various bands measured by Seleznev et al. [30], Tretyakov et al. [23], Devi et al. [24], Borkov et al. [9,27], Wójtewicz et al. [8], Balashov et al. [28], and this work. Bottom panel: The relative residuals from the Polynomial fitting are plotted.

potentially less reliable data did not unduly influence the fitting results. Therefore, we have re-fitted all the experimental data using a third-order polynomial ($a_w = A + B|m| + C|m|^2 + D|m|^3$), excluding the results of Devi et al. [24]. The fitting curve is shown as the red line in Fig. 6, with the parameters of the third-order polynomial being $A = 0.15785$, $B = -0.013073$, $C = 7.8430 \times 10^{-4}$ and $D = 1.1050 \times 10^{-5}$ as shown in Table 3. Within the $|m|$ interval, the standard deviation of the relative residuals for a_w (SDV profile) from the third-order polynomial is approximately 18%.

5. Conclusion

In this study, we measured 15 near-infrared transitions of CO using laser-locked cavity ring-down spectroscopy (LL-CRDS). This research

focuses primarily on the (3-0) vibrational band of CO, examining both the P and R branches with rotational quantum numbers J ranging from 25 to 35. The experiments were recorded under relatively low-pressure conditions (below 1333 Pa) where the Doppler line broadening was dominant. Collision broadening also significantly influenced the outcomes, facilitating accurate measurement of collision-related line shape parameters via spectral profile fitting. The SDV profile was applied in the analysis to derive the line shape parameters including the pressure-induced line broadening γ_0 and the speed-dependent line broadening γ_2 . To analyze the line shape parameters further, an empirical model Padé approximation was used. This method helped us to estimate broadening parameters related to its rotational quantum numbers and compare them with existing data. Our results extended the understanding of these parameters up to rotational quantum numbers as high

as 35, with a noted relative uncertainty of about 1%. For the speed-dependent parameter a_w , the relative residual of the fit using a third-order polynomial is approximately 17%. While the CRDS measurements were conducted at low pressures (below 1333 Pa), the derived self-broadening parameters (γ_0 and γ_2) and their extrapolation via the Padé approximation provide critical inputs for radiative transfer models at atmospheric pressures. The empirical model (Eq. (3)) incorporates historical multi-band data (Fig. 5), ensuring reliable predictions for high-J transitions. Although pressure-induced line shifts and velocity-changing collisions may become significant at higher pressures, the linear pressure dependence of Γ_0 dominates under typical atmospheric conditions. Our results, with uncertainties as low as 1%, will enhance the accuracy of existing databases and support high-fidelity simulations of Earth and planetary atmospheres in the 1.6 μm CO band. Additionally, this study primarily focuses on the self-broadening parameters of CO. However, for atmospheric remote sensing techniques, the broadening parameters of CO in the atmosphere are required, especially the air-broadening parameters. The results of this study provide high-precision self-broadening parameters of CO, laying a foundation for subsequent research on the broadening of CO in the atmosphere. In future research, the findings of this study can be combined with data from other research to establish a broadening model of CO in the atmosphere. This model can then be applied to the construction of atmospheric remote sensing techniques and environmental models, thereby promoting the development of the fields of atmospheric science and environmental protection.

CRedit authorship contribution statement

Q. Huang: Writing – review & editing, Writing – original draft, Validation, Investigation, Formal analysis, Data curation. **J. Wang:** Visualization, Validation, Investigation, Conceptualization. **J.-K. Li:** Conceptualization. **Z.-L. Nie:** Conceptualization. **A.-W. Liu:** Writing – review & editing, Conceptualization. **Y. Tan:** Writing – review & editing, Visualization, Supervision, Project administration, Methodology, Funding acquisition. **S.-M. Hu:** Writing – review & editing, Supervision, Project administration, Funding acquisition, Conceptualization.

Declaration of competing interest

The authors declare the following financial interests/personal relationships which may be considered as potential competing interests: Yan Tan reports financial support was provided by the Ministry of Science and Technology of China. Shui-Ming Hu reports a relationship with the National Natural Science Foundation of China that includes: funding grants. If there are other authors, they declare that they have no known competing financial interests or personal relationships that could have appeared to influence the work reported in this paper.

Acknowledgments

This work was supported by the Ministry of Science and Technology of China (Grant No. 2022YFF0606500, 2023ZD0301000), and the National Natural Science Foundation of China (Grant Nos. 12393822, 12393825, 22327801).

Data availability

Data will be made available on request.

References

- [1] Anne M. Thompson RJC. Possible perturbations to atmospheric CO, CH₄, and OH. *J Geophys Res: Atmos* 1986;91:10853–64. <http://dx.doi.org/10.1029/JD091D10p10853>.
- [2] Li S, Kim S, Lee H, Kenea ST, Kim JE, Chung C-Y, et al. Analysis of source distribution of high carbon monoxide events using airborne and surface observations in Korea. *Atmos Environ* 2022;289:119316. <http://dx.doi.org/10.1016/j.atmosenv.2022.119316>.
- [3] Jiang P, Chi X, Zhu Q, Cheng M, Gao H. Strong and selective isotope effect in the vacuum ultraviolet photodissociation branching ratios of carbon monoxide. *Nat Commun* 2019;10. <http://dx.doi.org/10.1038/s41467-019-11086-z>.
- [4] Connes P, Connes J, Kaplan LD, Benedict WS. Carbon monoxide in the Venus atmosphere. *Astrophys J* 1968;152:731–43. <http://dx.doi.org/10.1086/149590>.
- [5] Marq E, Mills FP, Parkinson CD, Vandaele AC. Composition and chemistry of the neutral atmosphere of Venus. *Space Sci Rev* 2018;214. <http://dx.doi.org/10.1007/s11214-017-0438-5>.
- [6] Owen T, Biemann K, Rushneck DR, Biller JE, Howarth DW, Lafleur AL. The composition of the atmosphere at the surface of mars. *J Geophys Res* 1977;82:4635–9. <http://dx.doi.org/10.1029/JS082i028p04635>.
- [7] Olsen KS, Lefèvre F, Montmessin F, Fedorova AA, Trokhimovskiy A, Baggio L, et al. The vertical structure of CO in the Martian atmosphere from the ExoMars trace gas orbiter. *Nat Geosci* 2021;14:67–71. <http://dx.doi.org/10.1038/s41561-020-00678-w>.
- [8] Wójtewicz S, Stec K, Masłowski P, Cygan A, Lisak D, Trawiński RS, et al. Low pressure line-shape study of self-broadened CO transitions in the (3-0) band. *J Quant Spectrosc Radiat Transfer* 2013;130:191–200. <http://dx.doi.org/10.1016/j.jqsrt.2013.06.005>.
- [9] Borkov YG, Solodov AM, Solodov AA, Petrova TM, Karlovets EV, Perevalov VI. Fourier transform co spectra near 1.6 μm . *J Quant Spectrosc Radiat Transfer* 2020;253. <http://dx.doi.org/10.1016/j.jqsrt.2020.107064>.
- [10] Hashemi R, Gordon IE, Adkins EM, Hodges JT, Long DA, Birk M, et al. Improvement of the spectroscopic parameters of the air- and self-broadened N₂O and CO lines for the HITRAN2020 database applications. *J Quant Spectrosc Radiat Transfer* 2021;271. <http://dx.doi.org/10.1016/j.jqsrt.2021.107735>.
- [11] Gordon IE, Rothman LS, Hargreaves RJ, Hashemi R, Karlovets EV, Skinner FM, et al. The hitran2020 molecular spectroscopic database. *J Quant Spectrosc Radiat Transfer* 2022;277:107949. <http://dx.doi.org/10.1016/j.jqsrt.2021.107949>.
- [12] Bielska K, Kyuberis AA, Reed ZD, Li G, Cygan A, Ciuryło R, et al. Submillimetre measurements and calculations of CO (3-0) overtone line intensities. *Phys Rev Lett* 2022;129. <http://dx.doi.org/10.1103/PhysRevLett.129.043002>.
- [13] Tan Y, Wang J, Zhao XQ, Liu AW, Hu SM. Cavity ring-down spectroscopy of the fifth overtone of CO. *J Quant Spectrosc Radiat Transfer* 2017;187:274–9. <http://dx.doi.org/10.1016/j.jqsrt.2016.10.003>.
- [14] Tan Y, Hua TP, Tang JD, Wang J, Liu AW, Sun YR, et al. Self- and N₂-broadening of CO in the low-pressure regime. *J Phys: Conf Ser* 2023;2439. <http://dx.doi.org/10.1088/1742-6596/2439/1/012007>, Institute of Physics.
- [15] Wang J, Hu C-L, Liu A-W, Sun YR, Tan Y, Hu S-M. Saturated absorption spectroscopy near 1.57 μm and revised rotational line list of ¹²C¹⁶O. *J Quant Spectrosc Radiat Transfer* 2021;270:107717. <http://dx.doi.org/10.1016/j.jqsrt.2021.107717>.
- [16] Huang Q, Tan Y, Yin R-H, Nie Z-L, Wang J, Hu S-M. Line intensities of CO near 1560 nm measured with absorption and dispersion spectroscopy. *Metrologia* 2024;61:065003. <http://dx.doi.org/10.1088/1681-7575/ad7ec0>.
- [17] Wang J, Sun YR, Tao LG, Liu AW, Hu SM. Communication: Molecular near-infrared transitions determined with sub-khz accuracy. *J Chem Phys* 2017;147:091103. <http://dx.doi.org/10.1063/1.4998763>.
- [18] Ngo N, Lisak D, Tran H, Hartmann J-M. An isolated line-shape model to go beyond the voigt profile in spectroscopic databases and radiative transfer codes. *J Quant Spectrosc Radiat Transfer* 2013;129:89–100. <http://dx.doi.org/10.1016/j.jqsrt.2013.05.034>.
- [19] Tran H, Ngo N, Hartmann J-M. Erratum to Efficient computation of some speed-dependent isolated line profiles [J. Quant. Spectrosc. Radiat. Transfer 129 (2013) 199–203]. *J Quant Spectrosc Radiat Transfer* 2014;134:104. <http://dx.doi.org/10.1016/j.jqsrt.2013.10.015>.
- [20] Cygan A, Lisak D, Wójtewicz S, Domysławska J, Hodges JT, Trawiński RS, et al. High-signal-to-noise-ratio laser technique for accurate measurements of spectral line parameters. *Phys Rev A* 2012;85. <http://dx.doi.org/10.1103/PhysRevA.85.022508>.
- [21] Nie Z, Wang X, Wang J, Yang Y, Hu C, Sun Y, et al. Calibration and application of optical manometer. *Vac Cryog* 2024;30:467–72. <http://dx.doi.org/10.12446/j.issn.1006-7086.2024.05.001>.
- [22] Cygan A, Kochanov RV, Rothman LS, Gordon IE. Introduction of water-vapor broadening parameters and their temperature-dependent exponents into the HITRAN database: Part I-CO₂, N₂O, CO, CH₄, O₂, NH₃, and H₂S. *J Geophys Res: Atmos* 2019;124:11580–94. <http://dx.doi.org/10.1029/2019JD030929>.
- [23] Tretyakov MY, Serov EA, Makarov DS, Vilkov IN, Golubiatnikov GY, Galanina TA, et al. Pure rotational R(0) and R(1) lines of CO in Ar baths: experimental broadening, shifting and mixing parameters in a wide pressure range versus ab initio calculations. *Phys Chem Chem Phys* 2022;25:1310–30. <http://dx.doi.org/10.1039/d2cp04917a>.

- [24] Devi VM, Benner DC, Smith MAH, Mantz AW, Sung K, Brown LR, et al. Erratum to spectral line parameters including temperature dependences of self- and air-broadening in the 2-0 band of CO at 2.3 μm [J Quant Spectrosc Radiat Transfer 113 (2012) 1013-33]. J Quant Spectrosc Radiat Transfer 2013;116:199–200. <http://dx.doi.org/10.1016/j.jqsrt.2012.11.020>.
- [25] Jacquemart D, Mandin J-Y, Dana V, Picqué N, Guelachvili G. A multispectrum fitting procedure to deduce molecular line parameters: Application to the 3-0 band of $^{12}\text{C}^{16}\text{O}$. Eur Phys J D - At Mol Opt Plasma Phys 2001;14:55–69. <http://dx.doi.org/10.1007/s100530170235>.
- [26] Picqué N, Guelachvili G, Dana V, Mandin J-Y. Absolute line intensities, vibrational transition moment, and self-broadening coefficients for the 3-0 band of $^{12}\text{C}^{16}\text{O}$. J Mol Struct 2000;517–518:427–34. [http://dx.doi.org/10.1016/S0022-2860\(99\)00267-7](http://dx.doi.org/10.1016/S0022-2860(99)00267-7).
- [27] Borkov YG, Solodov AM, Petrova TM, Solodov AA, Karlovets EV, Perevalov VI. Fourier transforms CO spectra near 1.19 μm . J Quant Spectrosc Radiat Transfer 2020;242. <http://dx.doi.org/10.1016/j.jqsrt.2019.106790>.
- [28] Balashov AA, Wójtewicz S, Domysławska J, Ciuryło R, Lisak D, Bielska K. CRDS line-shape study of the (7-0) band of CO. Spectrochim Acta - Part A: Mol Biomol Spectrosc 2024;312. <http://dx.doi.org/10.1016/j.saa.2024.124041>.
- [29] Esteki K, Predoi-Cross A, Povey C, Ivanov S, Ghoufi A, Thibault F, et al. Room temperature self- and h_2 -broadened line parameters of carbon monoxide in the first overtone band: Theoretical and revised experimental results. J Quant Spectrosc Radiat Transfer 2017;203:309–24. <http://dx.doi.org/10.1016/j.jqsrt.2017.04.008>.
- [30] Seleznev AF, Fedoseev GV, Koshelev MA, Tretyakov MY. Shape of collision-broadened lines of carbon monoxide. J Quant Spectrosc Radiat Transfer 2015;161:171–9. <http://dx.doi.org/10.1016/j.jqsrt.2015.04.011>.